Bioresource Technology

Kinetics characteristics and thermal behavior of co-pyrolysis of walnut shell-pyrolusite blends

--Manuscript Draft--

Manuscript Number:	BITE-D-20-03755
Article Type:	Original research paper
Keywords:	biomass-pyrolusite blends; co-pyrolysis; thermal behavior; kinetics characteristics; TGA
Corresponding Author:	jin chen kunming university of science and technology kunming, CHINA
First Author:	Kangqiang Li
Order of Authors:	Kangqiang Li
	Qi Jiang
	Guo Chen
	Lei Gao
	Jinhui Peng
	Quan Chen
	Sivasankar Koppala
	Mamdouh Omran
	jin chen
Abstract:	Combining biomass pyrolysis with microwave heating technologies provides a novel and efficient approach for low-grade pyrolusite reduction. The reduction behavior and pyrolysis kinetic characteristics of walnut shell-pyrolusite blends were explored. Results indicated that the optimal reduction parameters were: reduction temperature of 650 °C, holding time of 30 min, Mbio/More of 1.8:10, and microwave power of 1200 W. The co-pyrolysis characteristics of the blends included four stages: dehydration, pre-pyrolysis, intense pyrolysis and reduction, and slow pyrolysis and reduction. Fitting analysis based on Coats-Redfern method revealed that chemical reaction was the control step of the process of reducing pyrolusite by biomass, which the conclusion matched to the isothermal kinetic analysis results based on unreacted shrinking nuclear model. The activation energies and pre-finger factors were determined at 5.62 kJ·mol-1-16.69 kJ·mol-1 and 0.0426 min-1-0.515 min-1. The work provides sound references for promoting the industrial application of the combined method on minerals reduction.
Suggested Reviewers:	Mihajlo Gigov mihajlo.gigov@ribeograd.ac.rs
	Igor Plazl igor.plazl@fkkt.uni-lj.si
	Ján Vereš veres@saske.sk
	Chandrasekar Srinivasakannan srinivasa.chandrasekar@ku.ac.ae

The main highlights of this work are drawn as follows,

- Pyrolysis kinetic characteristics of walnut shell-pyrolusite blends were explored.
- Reduction behavior of co-pyrolysis of walnut shell-pyrolusite blends was investigated.
- The control step of the process of reducing pyrolusite by biomass was chemical reaction.
- Novel method with biomass pyrolysis and microwave heating merged to mineral reduction.

Kinetics characteristics and thermal behavior of co-pyrolysis of walnut shell-pyrolusite blends

Kangqiang Li [a], Qi Jiang [a], Guo Chen [a, b], Lei Gao [b], Jinhui Peng [a, b], Quan Chen [a], Sivasankar Koppala [c], Mamdouh Omran [d], Jin Chen [a, *]

[a] *Faculty of Metallurgical and Energy Engineering, Kunming University of Science and Technology, Kunming 650093, P.R. China.*

[b] *Key Laboratory of Green-Chemistry Materials in University of Yunnan Province, Yunnan Minzu University, Kunming 650500, P.R. China.*

[c] *Panjin Institute of Industrial Technology, Dalian University of Technology, Panjin 124221, Liaoning, P.R. China.*

[d] *Process Metallurgy Research Group, Faculty of Technology, University of Oulu, Finland.*

[*] Corresponding author: jinchen@kust.edu.cn

Abstract

Combining biomass pyrolysis with microwave heating technologies provides a novel and efficient approach for low-grade pyrolusite reduction. The reduction behavior and pyrolysis kinetic characteristics of walnut shell-pyrolusite blends were explored. Results indicated that the optimal reduction parameters were: reduction temperature of 650 °C, holding time of 30 min, M_{bio}/M_{ore} of 1.8:10, and microwave power of 1200 W. The co-pyrolysis characteristics of the blends included four stages: dehydration, pre-pyrolysis, intense pyrolysis and reduction, and slow pyrolysis and reduction. Fitting analysis based on Coats-Redfern method revealed that chemical reaction was the control step of the process of reducing pyrolusite by biomass, which the conclusion matched to the isothermal kinetic analysis results based on unreacted shrinking nuclear model. The activation energies and pre-finger factors were determined at 5.62 $kJ \cdot mol^{-1}$-16.69 $kJ \cdot mol^{-1}$ and 0.0426 min^{-1}-0.515 min^{-1}. The work provides sound references for promoting the industrial application of the combined method on minerals reduction.

Keywords: biomass-pyrolusite blends; co-pyrolysis; thermal behavior; kinetics characteristics; TGA

1 Introduction

The energy demand still maintains strong growth with the prosperous development of the world economy. Currently, global primary energy consumption mainly derives from coal (Abnisa and Wan Daud, 2014). However, coal is a well-known nonrenewable resource; meanwhile, its combustion renders 67% of nitrogen oxides (NO_x), 70% of soot and carbon

dioxide (CO_2) emissions and 90% of sulfur dioxides (SO_x), seriously aggravating greenhouse gas emissions and environmental pollution (Crutzen and Andreae, 1990; Tilman et al., 2006). Biomass is the only carbon-containing resource which can substitute fossil fuels, endowing green, rich and renewable characteristics, and it can be converted into tristate fuels and chemicals (including gas, liquid and solid) via biochemical conversion and chemical conversion processes (Corma et al., 2007; Ha et al., 2020). The biomass conversion technologies include microbial fermentation, pyrolysis, direct combustion, solidification, liquefaction, and gasification (Demirbas, 2000; Liu et al., 2018). More remarkably, biomass pyrolysis technology has aroused widespread attention in mineral reduction area, mainly using renewable biomass to replace conventional coal reductant and further to reduce the valuable metals in minerals. Cheng and Song used cornstalk and sawdust as reductants to process low-grade pyrolusite, and obtained the manganese recovery rates up to 90.20% and 97.71% under the roasting temperature of 500 °C-600 °C (Cheng et al., 2009; Song et al., 2010). Biomass endows the characteristics of carbon neutrality and low sulfur (S) and nitrogen (N) content; hence, during the biomass reduction process, no new carbon dioxide (CO_2) is generated, and the emissions of acid gases such as sulfur dioxides (SO_x) and nitrogen oxides (NO_x) are far lower than that by coal pyrolysis, greatly alleviating greenhouse effect and environmental pollution (Crutzen and Andreae, 1990; Tilman et al., 2006). Additionally, biomass resources are abundant and cheap, and the pyrolysis temperature of biomass (225 °C-500 °C) is much lower than that of coal pyrolysis (about 900 °C) (Abnisa and Wan Daud, 2014; Corma et al., 2007); therefore, compared with traditional reduction method, using biomass as the ore reducing agent can greatly reduce production costs and energy

consumption.

As an important national strategic resource, the application value of manganese (Mn) in the national economy and steel industry is irreplaceable (Jacob et al., 2020; Jung et al., 2018). However, 93.6% of manganese ore reserves in China is low-grade pyrolusite (Mn%<30%), meanwhile with those drawbacks such as high impurities, poor production concentration and poor processing performance, further rendering its quality and price are uncompetitive and incomparable with the imported high-grade manganese ore. Moreover, during the traditional carbothermal reduction method with coal as the reducing agent, some tricky problems also block the industrial development and production of low-grade pyrolusite, including high production cost and energy consumption and serious pollution (Ismail et al., 2010). Currently, with the increasing demand for manganese alloys, the synchronously increasing import pressure is driving the research and development of new process technologies of low-grade pyrolusite, which is expected to decrease the production cost and improve the comprehensive utilization level of low-grade pyrolusite, thereby alleviating the current import pressure and ensuring the sustainable production of manganese products.

Microwave heating is a new type of green and environmental-friendly heating method, endowing unparalleled features including selective heating, volume heating, timely response, fast heating rate, simple operation, clean production and green pollution-free (Chen et al., 2020a; Li et al., 2020a). Consequently, it is frequently applied as the substituted approach for traditional heating, especially in the fields of mineral pretreatment or reduction, ceramics or alloys materials preparation (Chen et al., 2020b; Li et al., 2020b). Ye at al. conducted the microwave carbothermal reduction experiments of low-grade pyrolusite, and obtained a

reduction ratio of 97.2% under shorter reduction time and lower processing temperature than that by traditional heating (Ye et al., 2014). During the heating process of magnetic materials such as ores, the thermal energy required for the reaction is produced by the coupling effect between microwave energy and the materials' dielectric loss, and directly supplied to reaction area, rather than through the heat transfer process from outside to inside as in conventional heating (Li et al., 2020c; Li et al., 2020d). Hence, the unique heating mechanism of microwave heating renders the effective reaction area and the reaction rate increased, further to result in the formation of microstructures with uniform distribution and small particle size, which in turn improves the performances of products (Li et al., 2020e; Li et al., 2020f). In addition, applying microwave heating on biomass pyrolysis process can effectively shorten the reaction time, increase the heating efficiency, and enhance the yield and performance of value-added products (Budarin et al., 2012; Motasemi and Afzal, 2013). Therefore, if the microwave heating technology and biomass pyrolysis technology are combined, referring to that replacing traditional coal by biomass as a reducing agent and replacing traditional heating by microwave heating as a heat source, it can be conjectured the reduction effect of this combined technology on low-grade pyrolusite is quite impressive.

The previous work first proposed the combined process to reduce low-grade pyrolusite, using walnut shell as biomass reducing agent and under microwave heating, and highlighted that the reduction ratio reached up to 92.01% after reduction at 650 °C for 30 min (Li et al., 2019a). Compared with traditional carbothermal reduction or microwave carbothermal reduction methods, the microwave-enhanced biomass pyrolysis reduction method rendered higher manganese reduction efficiencies and the reduction temperature decreased by 100 °C,

which the method is expected to realize low-energy production and efficient and clean utilization of low-grade pyrolusite. Therefore, to promote the industrial and commercial application of this combined method, the co-pyrolysis characteristics and reduction behavior of biomass-pyrolusite blends need to be further investigated, especially the reaction control step, pre-exponential factor (A) and activation energy (E_a). In the present study, the isothermal kinetic characteristics of low-grade pyrolusite reducing by biomass pyrolysis under microwave heating were explored; meanwhile, the non-isothermal kinetic characteristics and thermal behavior of co-pyrolysis of biomass-pyrolusite blends were studied using thermogravimetric analysis (TGA) and Coats-Redfern method; moreover, the reaction control step, pre-exponential factor and activation energy of the process of reducing pyrolusite by biomass were determined.

2 Materials and methods

2.1 Materials

The low-grade pyrolusite was derived locally from Daxin Manganese Mine of Chongzuo City, Guangxi Province, China. The component analysis of the pyrolusite sample was supplied by the affiliated analysis institution of Daxin Manganese Mine, determined based on the national standard ammonium nitrate (NH_4NO_3) method (GB/T1506-2002). As furnished in Table 1, the pyrolusite sample was in low-grade (T_{Mn}%<30%), and contained high contents of iron (7.76%) and silicon (25.83%). Meanwhile, it can be abstracted from the XRD pattern that the crystal structures of pyrolusite sample mainly included MnO_2 (i.e. manganese oxide phase, JCPDS: 44-0141), $(Fe, Mn)_2SiO_4$ (i.e. olivine phase, JCPDS: 12-0220), and SiO_2 (i.e.

quartz phase, JCPDS: 46-1045) (see Supplementary data).

Walnut shell is abundant in Yunnan Province (P.R. China) and locally available in Chuxiong Nutshell Processing Factory. Meanwhile, the recent studies have confirmed that walnut shell-pyrolusite blends endow superior microwave-absorbing ability (Li et al., 2019b; Li et al., 2019c), and walnut shell presents a good reduction effect for low-grade pyrolusite under microwave heating (Li et al., 2019a). Thus, it was chosen as the biomass reducing agent to conduct the kinetic experiments of low-grade pyrolusite reducing by biomass under microwave heating. The composition analytical results of walnut shell were furnished in Table 2, including proximate analysis and ultimate analysis results determined by Advanced Analysis and Measurement Center of Yunnan University.

2.2 Procedure

The as-received samples of walnut shell and pyrolusite were through drying, grinding and screening. After screening, the obtained powder samples with a particle size of -100 mesh-+130 mesh were selected out to be mixed with different mixing ratios (M_{bio}/M_{ore}) to form five walnut shell-pyrolusite blends, wherein the mass of pyrolusite was constant at 20.0 g, and the mass of walnut shell varied with M_{bio}/M_{ore} value, including 1.2:10, 1.4:10, 1.6:10, 1.8:10, and 2.0:10. And then the powder tablet press (Model: 769YP-24B) was used to form spheroidal samples of five walnut shell-pyrolusite blends, further to promote the completion of reducing low-grade pyrolusite using biomass under microwave heating. After pelletizing, the spheroidal samples were introduced into a microwave vacuum heating furnace (Model: MYWAVE) to conduct the kinetic experiments of pyrolusite reducing using walnut shell under microwave heating. During the kinetic experiments, reduction temperature varied from

450 °C, 500 °C, 550 °C, 600 °C, and 650 °C; holding time ranged from 0 min, 5 min, 10 min, 15 min, 20 min, 25 min, 30 min, 45 min, and 60 min; and microwave powder varied from 600 W, 800 W, 1000 W, 1200 W, and 1400 W. After reaching the set experiment parameters, the microwave heated spheroidal samples were moved quickly into the crucible, with tin foil sealed to avoid the influence of air oxidation on the subsequent reduction indexes analysis of low-grade pyrolusite. The kinetic experiments were carried out for the reduction indexes analysis and isothermal kinetic analysis of walnut shell-pyrolusite blends.

In addition, thermogravimetric measurements for pyrolusite, walnut shell and five walnut shell-pyrolusite blends were conducted for the thermal behavior analysis and non-isothermal kinetic analysis of co-pyrolysis of walnut shell-pyrolusite blends. The thermogravimetric measurements were performed using METTLER TOLEDO TGA/DSC1/1600 analyzer, under the measurement conditions of the powder samples with a particle size of -100 mesh-+130 mesh, test temperature ranging from 30 °C to 900 °C with 30 K/min of the heating rate, 60 mL/min of argon (Ar) as the test atmosphere.

2.3 Pyrolysis kinetics

Kinetic characteristics of biomass pyrolysis are usually determined by isoconversional approaches. In isoconversional approaches, there is absent of the relationship between the reaction mechanism with the temperature and heating rate (Sun et al., 2012). Generally, the non-isothermal conversion rate of solid samples can be defined as (Ma and Li, 2012):

$$\frac{dX}{dt} = kf(X) \tag{1}$$

Where X is the conversion rate, expressed as:

$$X = \frac{W_i - W}{W_i - W_f} \tag{2}$$

Where W, W_i and W_f represent the initial weight, instantaneous weight and final weight of the

sample, respectively.

In the Arrhenius equation, the definition of the reaction rate constant (k) is written as:

$$k = Aexp(\frac{-E_a}{RT}) \quad (3)$$

Where A, R, E_a, and T are called the pre-finger factor (s^{-1}), molar gas constant (8.314 $J \cdot mol^{-1} \cdot K^{-1}$), activation energy ($J \cdot mol^{-1}$), and reaction temperature (K), respectively.

The function $f(X)$ is related to the conversion rate (X), written as:

$$f(X) = (1 - X)^n \quad (4)$$

Therefore, substituting Eq. (3)~(4) into Eq. (1), the following equation can be obtained as:

$$\frac{dX}{dt} = Aexp(\frac{-E_a}{RT})(1 - X)^n \quad (5)$$

3 Results and discussion

3.1 Reduction indexes analysis

Reduction quality of pyrolusite using biomass under microwave heating is usually determined by the reduction rate, expressed as:

$$\eta_{Mn} = \frac{M_2}{M_1} \quad (6)$$

Where η_{Mn} is the reduction rate; M_1 is the weight percentage of Mn^{4+} in raw pyrolusite sample; M_2 is the weight percentage of Mn^{4+} reduced into Mn^{2+} by biomass pyrolysis. The analytical results of Mn^{4+} and Mn^{2+} in pyrolusite samples before and after kinetic experiments were supplied by the affiliated analysis institution of Daxin Manganese Mine, determined based on the national standard ammonium nitrate (NH_4NO_3) method (GB/T1506-2002). During the kinetic experiments, the effects of experimental parameters on the reduction rate of low-grade pyrolusite were explored, including reduction temperature, mixing ratio

(M_{bio}/M_{ore}), holding time, and microwave power, and the obtained experimental data were illustrated in Fig. 1.

Effects of reduction temperature and M_{bio}/M_{ore} on the reduction rate were depicted in Fig. 1(a), wherein the microwave power and holding time was constant at 1200 W and 30 min, respectively. As illustrated in Fig. 1(a), when M_{bio}/M_{ore} value was constant at 1.2:10, as the reduction temperature increased from 450 °C to 650 °C, the reduction rate (η_{Mn} value) correspondingly improved from 44.06% to 64.87%. Similarly, as M_{bio}/M_{ore} value increased from 1.2:10 to 1.8:10, the change trends of η_{Mn} value with the reduction temperature were the same, all showing a positive growth trend, with η_{Mn} value improving from 45.96% to 80.93%, from 48.82% to 85.59%, and from 54.55% to 92.01%. Moreover, when M_{bio}/M_{ore} value increased to 2.0:10, an inflection point of η_{Mn} value appeared at 600 °C. Specifically, the η_{Mn} value improved from 56.24% to 79.18% with reduction temperature improving from 450 °C to 600 °C; however, the η_{Mn} value decreased from 79.18% at 600 °C to 77.14%, with reduction temperature continuously increasing to 650 °C. The η_{Mn} value in manganese plant must be greater than 88% to enter the subsequent electrolysis workshop. Therefore, it can be determined from the above analysis that the optimal reduction temperature was 650 °C.

The relationship between mixing ratio (M_{bio}/M_{ore}) and reduction rate was not clear, with an inflection point of η_{Mn} value appeared at 600 °C, as shown in Fig. 1(a). Therefore, the single factor influence experiments of the mixing ratio on the reduction rate under various microwave powers were supplemented, expecting to explore the optimal mixing ratio (M_{bio}/M_{ore}) parameter. Effects of mixing ratio on the reduction rate under different reduction temperatures were illustrated in Fig. 1(b), wherein the microwave power and holding time

was constant at 1000 W and 30 min, respectively. As depicted in Fig. 1(b), whether the reduction temperature was 450 °C or 650 °C, inflection points of η_{Mn} value appeared with M_{bio}/M_{ore} value increasing to 1.8:10. Specifically, controlling reduction temperature constant at 450 °C, as M_{bio}/M_{ore} increased from 1.2:10 to 1.8:10 and 2.0:10, η_{Mn} value improved from 81.79% to 88.67% and then decreased to 81.71%. Similarly, maintaining reduction temperature at 650 °C, as M_{bio}/M_{ore} increased from 1.2:10 to 1.8:10 and 2.0:10, the η_{Mn} value improved from 77.30% to 97.08% and then decreased to 87.09%. Additionally, as presented in Fig. 1(a), at a temperature higher than 550 °C, the ηMn values under a M_{bio}/M_{ore} value of 1.8:10 were all higher than that under a M_{bio}/M_{ore} value of 2.0:10. In summary, the optimal mixing ratio (M_{bio}/M_{ore} value) was determined to be 1.8:10.

Effects of holding time on the reduction rate were depicted in Fig. 1(c), wherein the microwave power, holding time, and mixing ratio were constant at 1200 W, 30 min and 1.8:10, respectively. As shown in Fig. 1(c), as holding time increased from 0 min to 30 min, η_{Mn} value improved from 88.40% to 92.01%; at holding time exceeding 30 min, η_{Mn} value decreased to 91.36% with a holding time 45 min and 91.45% with 60 min. In summary, the optimal holding time was determined to be 30 min.

Effects of microwave power on the reduction rate were illustrated in Fig. 1(d), wherein the microwave power, holding time, reduction temperature, and mixing ratio were constant at 30 min, 650 °C, and 1.8:10, respectively. As observed from Fig. 1(d), as heating power improved from 600 W to 1200 W, η_{Mn} value increased from 79.83% to 92.01%; as microwave power increased to 1400 W, η_{Mn} value decreased to 87.98% instead. Therefore, the optimal microwave power was determined to be 1200 W.

3.2 Isothermal kinetic analysis

3.2.1 Isothermal kinetic model

The reactions occurred in biomass-pyrolusite blends mainly include solid-solid and gas-solid reduction reactions between metal compounds and biomass pyrolysis products, and gasification reaction of carbon (biochar produced by biomass pyrolysis) (Li et al., 2019a; Zhang et al., 2013a). Secondly, the generation temperature of biochar in biomass pyrolysis products is much higher than that of gas components; meanwhile, the reaction activation energy to generate biochar is the highest, the reaction activation energy about bio-oil is in the center, with the reaction activation energy about gas components being lowest. Moreover, with temperature rising, the yield of biochar decreases, and the yield of combustible gas improves (Abnisa and Wan Daud, 2014; Corma et al., 2007). Additionally, the main metal compound in the pyrolusite sample was MnO_2 phase (see Supplementary data), and carbon monoxide (CO) is the representative gas product produced by biomass pyrolysis (Li et al., 2019a; Zhang et al., 2013a). Therefore, to simplify the kinetics analysis, only the kinetic characteristics of gas-solid reduction reactions between MnO_2 phase and carbon monoxide (CO) in biomass-pyrolusite blends were investigated, without taking the solid-solid reduction reaction of MnO_2 phase and biochar and gasification reaction of biochar into account. The reactions involved were as follows:

$$MnO_2(s)+CO(g)=Mn_2O_3(s)+CO_2(g) \quad (7)$$

$$3Mn_2O_3(s)+CO(g)=2Mn_3O_4(s)+CO_2(g) \quad (8)$$

$$Mn_3O_4(s)+CO(g)=3MnO(s)+CO_2(g) \quad (9)$$

$$MnO(s)+CO(g)=Mn(s)+CO_2(g) \quad (10)$$

Combining with Eq. (7)- Eq. (10), it can be concluded that the reactions in biomass-pyrolusite blends are gas-solid reduction reactions. Therefore, to guarantee the reaction process of reducing low-grade pyrolusite by biomass pyrolysis conform to the unreacted shrinking nuclear model, the following assumptions need to be supplemented (Hua, 2004; Li, 2005): (1) MnO_2 phase in pyrolusite sample has a single particle size, a dense spherical shape and the same chemical properties in all directions; (2) After reduction process, the product layer has a porous structure, and the reaction core becomes smaller and smaller with the reactions proceeding; (3) In biomass pyrolysis products, only carbon monoxide (CO) reacts with MnO_2 phase. Therefore, combining the above analysis and assumptions on the reduction process of low-grade pyrolusite with biomass and the five series steps of shrinking unreacted nuclear model, it can be concluded that the limiting link involved in this reaction process is diffusion control or chemical reaction control (Hua, 2004; Li, 2005).

Based on the above assumptions, if the reaction process of reducing low-grade pyrolusite by biomass pyrolysis is controlled by chemical reaction (Eq. (11), external diffusion control (Eq. (12) and internal diffusion control (Eq. (13), the dynamic equations are expressed correspondingly as follows:

$$1-(1-a)^{1/3}=k_1t \quad (11)$$

$$1-2a/3-(1-a)^{2/3}=k_2t \quad (12)$$

$$1-(1-a)^{2/3}=k_2t \quad (13)$$

Where a is the reduction rate; t is the reaction time, s; k_1 and k_2 are the apparent rate constants of chemical reaction and diffusion reaction, s^{-1}.

3.2.2 Fitting analysis of isothermal kinetic model

The kinetic control step of a reaction process is evaluated according to the fitting curve between reaction kinetic equations and time (t). Summarised from the above reduction indexes analysis, the optimal experimental parameters were drawn as follows: reduction temperature of 650 °C, M_{bio}/M_{ore} of 1.8:10, microwave power of 1200 W, and holding time of 30 min. It is worthy to note that in the kinetic experiments, microwave furnace operates in automatic mode; hence, for the same material and target temperature (650 °C), the time for the material to reach 650 °C is the same under microwave heating. Therefore, when considering the relationship between the kinetic equation and the time equivalent (t), the parameter value of holding time can be used instead of the time equivalent (t). As illustrated in Fig. 1 (c), with holding time exceeding 30 min, the manganese reduction rate decreased. Therefore, the reduction rates obtained under the condition of holding time less than or equal to 30 min were substituted into the kinetic equations (Eq. (11)~(13)) for fitting, and the fitted results were presented in Fig. 2.

As observed from Fig. 2, each control equation presented a linear relationship with time. Therefore, it is necessary to compare the fitting effects of each dynamic equation. Regarding the chemical reaction control equation, the fitting effects of using all 6 data (referring to the duration regime of 5 min-30 min) and the first 5 data (referring to the duration regime of 5 min-25 min) were detailed as follows: the fitting degree (R_2) was 0.88577 and 0.91193, respectively, with good linear fit effects; in addition, F-test value (Prob>F) was 0.00323 and 0.00735, respectively, which were both far less than 0.05, indicating the high level of credibility. Secondly, for the external diffusion control equation, the fitting degree (R_2) was

0.87895 and 0.90395, respectively, with good linear fit effects; additionally, F-test value was 0.00305 and 0.00710, respectively, both far less than 0.05, indicating the high level of credibility. Similarly, for the internal diffusion control equation, the fitting degree (R_2) was 0.88416 and 0.90250, respectively, with good linear fit effects; additionally, F-test value was 0.00333 and 0.00728, respectively, both far less than 0.05, indicating the high level of credibility. Combining the fitting effects of the three kinetic control equations, it can be preliminarily determined that the reaction process of pyrolusite reducing by biomass pyrolysis under microwave heating was controlled by chemical reactions, which the finding was consistent with that of previous related studies (Ye et al., 2018; Zhao et al., 2010; Zhang et al., 2013a).

3.3 Thermal behavior analysis

Thermogravimetric analysis (TGA) can expose the weight loss of samples with temperature (Lu et al., 2013), and the findings obtained from thermogravimetric analysis can contribute to analyze the reaction kinetics, further to explore the reaction mechanisms. TGA analysis has been widely applied to investigate the kinetic characteristics and thermal behavior of co-pyrolysis of the blends of biomass with other substances (Azizi et al., 2017; Lu et al., 2013; Xiang et al., 2018).

3.3.1 Pyrolysis characteristics of pyrolusite and walnut shell

TGA-DTG curves of low-grade pyrolusite and walnut shell were plotted in Fig. 3. As shown in Fig. 3(a), the thermal characteristics of low-grade pyrolusite contained three stages: (1) The first stage (30 °C-400 °C), was mainly represented by the removal of adsorption water and crystal water of low-grade pyrolusite. (2) The second stage (400 °C-700 °C), mainly arose

the decomposition reaction of MnO_2 phase in low-grade pyrolusite. The endothermic peaks at 550.0 °C and 581.7 °C corresponded to the decomposition reaction of $4MnO_2(s) \rightarrow 2Mn_2O_3(s) + O_2(g)$, as marked in Fig. 3(a). (3) The third stage (700 °C-800 °C), mainly occurred the decomposition reaction of $CaCO_3$ phase in low-grade pyrolusite, wherein the decomposition reaction equation is expressed as $CaCO_3(s) \rightarrow CaO(s) + CO_2(g)$.

For walnut shell, as depicted in Fig. 3(b), the pyrolysis process of walnut shell included four stages: (1) The first stage (30 °C-100 °C) was the dehydration stage. During this temperature period, the water molecules in walnut shell material evaporated, and the chemical composition of the biomass material almost unchanged. (2) The second stage (100 °C-250 °C) was the pre-pyrolysis stage. At this temperature regime, the bound water removed, glass transitions and depolymerization reactions also arose. The chemical composition began to change, unstable hemicellulose was pyrolyzed into CO, CO_2 and acetic acid (Mehrabian and Scharler, 2012), with the obvious thermal effect observed in Fig. 3(b). (3) The third stage (250 °C-430 °C) was the curing pyrolysis stage. In the pyrolysis stage, various substances were generated through multiplex physicochemical reactions, wherein the solid products produced were mainly biochar, formed through rearrangement reactions and free radical reactions; the liquid products involved methanol and acetic acid, and the gas products included CO, H_2, CO_2 and CH_4, etc., generated by the gradual cleavage of C-C bonds and glycosidic bonds. Meanwhile, the hydrocarbon groups on the branch chain and low molecular volatile products were produced by the gradual cleavage of C-C bonds and C-O bonds. (4) The fourth stage (>430 °C) was the carbonization stage. In this stage, the remained cellulose and lignin were pyrolyzed, and the by-products (such as coke and tar) underwent secondary

cracking. The main feature was the breakage of the C-C bonds to produce porous coke with a stable graphite structure, and the breakage of the C-H bonds to form small molecule gases (Lapuerta and Hernández, 2004); meanwhile, the remaining volatile substances in the coke were released to the outer layer and finally formed biochar.

3.3.2 Co-pyrolysis characteristics of walnut shell-pyrolusite blends

The TGA-DTG curves of five walnut shell-pyrolusite blends were illustrated in Fig. 4, determined under the heating rate of 30 K/min and different mixing ratios of 1.2:10, 1.4:10, 1.6:10, 1.8:10, and 2.0:10.

As presented in Fig. 4, the changing trends of five TGA-DTG curves were similar, and the co-pyrolysis characteristics of walnut shell-pyrolusite blends contained four stages: (1) The first stage (30 °C-150 °C), mainly occurred the removal of absorption water of the blends, with the endothermic peaks arose at 96.6 °C, 96.8 °C, 69.1 °C, 85.3 °C, and 70.4 °C, respectively. (2) The second stage (150 °C-310 °C), mainly occurred the pre-pyrolysis process of walnut shell to generate reducing gas components as the main products; followed by the metal oxides in pyrolusite were reduced by hydrogen (H_2), complying with the conversion order: $MnO_2 \rightarrow Mn_2O_3 \rightarrow Mn_3O_4 \rightarrow MnO$ (see Supplementary data). (3) The third stage (310 °C-440 °C), corresponded to the main pyrolysis stage of walnut shell and the intensive reduction stage of pyrolusite sample. During this stage, walnut shell was through primary cracking and secondary cracking to generate biochar, tar, and gas, with the sufficient reducing components to react with manganese and iron oxides, complying with the conversion order: $MnO_2 \rightarrow Mn_2O_3 \rightarrow Mn_3O_4 \rightarrow MnO$ and $Fe_2O_3 \rightarrow Fe_3O_4$ (see Supplementary data). (4) The four stage (>440 °C), was mainly manifested by the slow reduction of remaining unreduced

manganese oxides and the conversion of $Fe_3O_4 \rightarrow FeO$. The more detailed information was provided in the recent work (Li et al., 2019a; Li et al., 2019b). Moreover, the differences in heating rate will cause the shift of peak temperature, and the node temperature between the second and third stages differed nearly 10 °C, with 290 °C, 300 °C and 310 °C determined under the heating rate of 10 K/min, 20 K/min and 30 K/min (see Supplementary data). The finding was also proved by the recent work (Li et al., 2019a; Li et al., 2019b).

3.3.3 Synergetic interaction between pyrolusite and walnut shell

To expose the synergistic interaction between pyrolusite and walnut shell, the difference (ΔW) between the experimentally measured and the calculated thermogravimetric data is defined as (Cai et al., 2008; Zhang et al., 2016):

$$\Delta W = W_{mixture} - (\chi_1 W_1 + \chi_2 W_2) \quad (14)$$

Where $W_{mixture}$ is the weight loss of the walnut shell-pyrolusite blend; W_i is the weight loss of each substance under the same measurement conditions; χ_i is the weight fraction of each substance in the blend.

The ΔW deviations of five walnut shell-pyrolusite blends with different mixing ratios were plotted in Fig. 5. As shown in Fig. 5(a), the ΔW deviation of five TGA curves presented the same changing trend: ΔW value decreased first, next increased, then declined again, and then rose again, finally fell again. In addition, for the ΔW deviation of five DTG curves, the same changing trend was also observed from in Fig. 5(b). Furthermore, as presented in Fig. 5(a), the ΔW deviations of TGA curves of five walnut shell-pyrolusite blends all had a minimum value at temperatures between 400 °C and 600 °C, and the main reaction stage of low-grade pyrolusite reducing by biomass also occurred at the temperature range (Li et al., 2019a; Li et al., 2019c). Therefore, the weight loss of walnut shell-pyrolusite blends at the temperature regime can be regarded as the process degree of the reduction reaction of

pyrolusite by biomass pyrolysis.

The comparison of the maximum relative error at 400 °C-600 °C between the calculated and experimental TGA curves of five walnut shell-pyrolusite blends was listed in Table 3. Specifically, under a M_{bio}/M_{ore} value of 1.2:10, the minimum value was -3.721, appearing at 522.4 °C, and the corresponding maximum relative error was 4.474%; under a M_{bio}/M_{ore} value of 1.4:10, the minimum value appeared at 524.0 °C with a value of -5.476, the corresponding maximum relative error was 6.814%; under a M_{bio}/M_{ore} value of 1.6:10, the minimum value and the maximum relative error were -4.932 and 6.191%, appearing at 536.0 °C; under a M_{bio}/M_{ore} value of 1.8:10, the minimum value and the maximum relative error were -3.562 and 3.641%, appearing at 535.8 °C; besides, under a M_{bio}/M_{ore} value of 2.0:10, the minimum value and the maximum relative error were -2.939 and 4.500%, appearing at 535.9 °C, as listed in Table 3. Table 4 illustrated the comparison of residues between the experimental and calculated TGA curves of five walnut shell-pyrolusite blends. As presented in Table 4, the residues of five walnut shell-pyrolusite blends were very close, with the experimental and calculated residue values between 73 wt%-77 wt% and 78 wt%-82 wt%.

3.4 Non-isothermal kinetic analysis

3.4.1 Non-isothermal kinetic model

Coats-Redfern method has occupied an important application value in the non-isothermal kinetic analysis (Coats and Redfern, 1964; Lu et al., 2013; Xiang et al., 2018). If the heating rate is constant ($\beta = \frac{dT}{dt}$), Eq. (5) can be reorganized as:

$$\frac{dX}{dT} = (\frac{1}{\beta})Aexp(\frac{-E_a}{RT})(1-X)^n \quad (15)$$

Based on the Coats-Redfern method, the logarithmic expression of Eq. (15) is:

$$\ln[\frac{-\ln(1-X)}{T^2}] = \ln\frac{AR}{\beta E_a}\left[1-\frac{2RT}{E}\right]-\frac{E_a}{RT} \qquad if\ n=1 \quad (16)$$

Or

$$\ln[\frac{-(1-X)^{1-n}}{(1-n)\times T^2}] = \ln\frac{AR}{\beta E_a}\left[1-\frac{2RT}{E}\right]-\frac{E_a}{RT} \qquad if\ n \neq 1 \tag{17}$$

The value of 2RT/E in most reactions is very small (i.e. 2RT/E<<1), so Eq. (16) and Eq. (17) can be simplified as:

$$\ln[\frac{-\ln(1-X)}{T^2}] = \ln\frac{AR}{\beta E_a}-\frac{E_a}{RT} \qquad if\ n = 1 \tag{18}$$

Or

$$\ln[\frac{-(1-X)^{1-n}}{(1-n)\times T^2}] = \ln\frac{AR}{\beta E_a}-\frac{E_a}{RT} \qquad if\ n \neq 1 \tag{19}$$

The curves of $\ln[\frac{-\ln(1-X)}{T^2}]$ and $\ln[\frac{-(1-X)^{1-n}}{(1-n)\times T^2}]$ versus 1/T are linearly related. Therefore, the pre-finger factor (A) and activation energy (E_a) can be obtained according to the intercept and slope of the regression line.

3.4.2 Fitting analysis of non-isothermal kinetic model

The process of reducing manganese ore by biomass pyrolysis can be considered as the linearly superimposed processes of reducing manganese ore by the three main components of biomass, referring to cellulose, hemicellulose and lignin (Zhang et al., 2013a; Zhang et al., 2013b). Therefore, the first-order kinetic equation based on Coats-Redfern method was applied for the kinetic analysis of co-pyrolysis of walnut shell-pyrolusite blends. In addition, regardless of whether the heating rate of the thermogravimetric test was 10 K/min, 20 K/min or 30 K/min, the peaks of the second and third stages of thermogravimetric characteristics of walnut shell-pyrolusite blends all appeared at temperatures between 250 °C and 400 °C, and the main reaction stage of low-grade pyrolusite reducing by biomass also occurred at the temperature range (see Supplementary data). To simplify the calculation, the X values (the conversion rate) obtained through processing the thermogravimetric data at 250 °C-400 °C were substituted into Eq. (5), the fitting curves of $\ln[\frac{-\ln(1-X)}{T^2}]$ versus 1/T were illustrated in Fig. 6.

As observed from Fig. 6, the fitting effects between the thermogravimetric data of five walnut shell-pyrolusite blends and the Coats-Redfern first-order kinetic equation were all very good, with all the fitting degree (R_2) more than 0.995. The fitted results indicated the reaction process of pyrolusite reducing by walnut shell was controlled by chemical reactions, which the finding consolidated the above conclusion obtained from isothermal kinetic analysis, that is, the reaction process of pyrolusite reducing by biomass pyrolysis under microwave heating was controlled by chemical reactions. The conclusion was also matched to that of previous related studies (Ye et al., 2018; Zhang et al., 2013a).

Kinetics parameters of reducing pyrolusite by walnut shell were presented in Table 5. Observed from Table 5, as the mixing ratio (M_{bio}/M_{ore} value) improved, the E_a and A values simultaneously presented the trend of decreasing first and then increasing. In detail, with the mixing ratio increasing from 1.2:10 to 1.8:10, the E_a value decreased from 16.68 $kJ \cdot mol^{-1}$ to 5.62 $kJ \cdot mol^{-1}$, and the A value decreased from 0.41 min^{-1} to 0.0426 min^{-1}; with the mixing ratio continuously increasing to 2.0:10, the E_a value counterly increased from 5.62 $kJ \cdot mol^{-1}$ to 16.69 $kJ \cdot mol^{-1}$, and the A value also improved from 0.0426 min^{-1} to 0.515 min^{-1}. The smaller the activation energy of the reaction, the easier the reaction is to proceed. As observed from Table 5, the E_a value was the lowest under a mixing ratio of 1.8:10, indicating that the reaction of reducing low-grade pyrolusite by biomass pyrolysis at this mixing ratio processed the most easily. Thereby, the reduction efficiency of pyrolusite by walnut shell was the highest under the same mixing ratio of 1.8:10, which this conclusion was coincident with the finding that the optimal mixing ratio of 1.8: 10, determined by the above quality indexes analysis (Fig. 1).

4 Conclusions

In this work, the kinetic characteristics and thermal behavior of co-pyrolysis of walnut shell-pyrolusite blends were investigated. Results indicated the co-pyrolysis characteristics of the blends contained four stages: 30 °C-150 °C, 150 °C-310 °C, 310 °C-440 °C, >440 °C, with good synergetic interaction. The reaction process of low-grade pyrolusite reducing by biomass pyrolysis under microwave heating was controlled by chemical reaction, which the finding was consolidated by the non-isothermal kinetic analysis, with all R_2 value more than 0.995. The E_a and A value of reducing low-grade pyrolusite by walnut shell were 5.62 $kJ \cdot mol^{-1}$-16.69 $kJ \cdot mol^{-1}$ and 0.0426 min^{-1}-0.515 min^{-1}.

Acknowledgments

Financial supports from the National Natural Science Foundation of China (No: U1802255), and Innovative Research Team (in Science and Technology) in University of Yunnan Province were sincerely acknowledged.

Appendix A. Supplementary data

E-supplementary data for this work can be found in e-version of this paper online.

References

1. Abnisa, F., Wan Daud, W.M.A., 2014. A review on co-pyrolysis of biomass: An optional technique to obtain a high-grade pyrolysis oil. Energy Conversion and Management. 87, 71-85. https://doi.org/10.1016/j.enconman.2014.07.007.

2. Azizi, K., Moraveji, M.K., Najafabadi, H.A., 2017. Characteristics and kinetics study of simultaneous pyrolysis of microalgae Chlorella vulgaris, wood and polypropylene through TGA. Bioresource Technology. 243, 281-291. https://doi.org/10.1016/j.biortech.2017.06.155.
3. Budarin, V., Gronnow, M., Clark, J.H., Luque, R., 2012. Low temperature microwave-assisted vs conventional pyrolysis of various biomass feedstocks. Journal of Natural Gas Chemistry. 21(3), 270-274. https://doi.org/10.1016/S1003-9953(11)60364-2.
4. Cai, J.Q, Wang, Y.P., Zhou, L.M., Huang, Q.W., 2008. Thermogravimetric analysis and kinetics of coal/plastic blends during co-pyrolysis in nitrogen atmosphere. Fuel Processing Technology. 89 (1), 21-27. https://doi.org/10.1016/j.fuproc.2007.06.006.
5. Chen, G., Jiang, Q., Li, K.Q., He, A.X., Peng, J.H., Omran, M., Chen, J., 2020a. Simultaneous removal of Cr(III) and V(V) and enhanced synthesis of high-grade rutile TiO_2 based on sodium carbonate decomposition. Journal of Hazardous Materials. 388, 122039. https://doi.org/10.1016/j.jhazmat.2020.122039.
6. Chen, G., Li, K.Q., Jiang, Q., Li, X.P., Peng, J.H., Omran, M., Chen, J., 2020b. Microstructure and enhanced volume density properties of FeMn78C8.0 alloy prepared via a cleaner microwave sintering approach. Journal of Cleaner Production. 262, 121364. https://doi.org/10.1016/j.jclepro.2020.121364.
7. Cheng, Z., Zhu, G.C., Zhao, Y.N., 2009. Study in reduction-roast leaching manganese from low-grade manganese dioxide ores using cornstalk as reductant. Hydrometallurgy. 96 (1-2), 176-179. https://doi.org/10.1016/j.hydromet.2008.08.004.
8. Coats, A.V., Redfern, J.P., 1964. Kinetic parameters from thermogravimetric data. Nature. 201, 68-69. https://doi.org/10.1038/201068a0.

9. Corma, A., Iborra, S., Velty, A., 2007. Chemical routes for the transformation of biomass into chemicals. Chemical Reviews. 107 (6), 2411-502. https://doi.org/10.1021/cr050989d.

10. Crutzen, P.J., Andreae, M.O., 1990. Biomass burning in the tropics: Impact on atmospheric chemistry and biogeochemical cycles. Science. 250 (4988), 1669-1678. https://doi.org/10.1126/science.250.4988.1669.

11. Demirbas, A., 2000. Mechanism of liquefaction and pyrolysis reactions of biomass. Energy Conversion and Management. 41 (6), 633-646. https://doi.org/10.1016/S0196-8904(99)00130-2.

12. Ha, G., El-Dalatony, M.M., Kurade, M.B., Salama, E., Basak, B., Kang, D.H., Roh, H., Lim, H., Jeon, B., 2020. Energy-efficient pretreatments for the enhanced conversion of microalgal biomass to biofuels. Bioresource Technology. 309, 123333. https://doi.org/10.1016/j.biortech.2020.123333.

13. Hua, Y.X., 2004. Metallurgical Process Dynamics. Metallurgical Industry Press, Beijing. pp. 144-156.

14. Ismail, A. A., Ali, E.A., Ibrahim, I.A., Ahmed, M.S., 2010. A comparative study on acid leaching of low grade manganese ore using some industrial wastes as reductants. Canadian Journal of Chemical Engineering. 82 (6), 1296-1300. https://doi.org/10.1002/cjce.5450820618.

15. Jacob, R., Sankaranarayanan, S.R., Babu, S.P.K., 2020. Recent advancements in manganese steels-A review. Materials Today: Proceedings. https://doi.org/10.1016/j.matpr.2020.01.296.

16. Jung, K.W., Lee, S.Y., Lee, Y.J., 2018. Facile one-pot hydrothermal synthesis of cubic spinel-type manganese ferrite/biochar composites for environmental remediation of

heavy metals from aqueous solutions. Bioresource Technology. 261, 1-9. https://doi.org/10.1016/j.biortech.2018.04.003.

17. Lapuerta, M., Hernández, J.J., Rodríguez, J., 2004. Kinetics of devolatilisation of forestry wastes from thermogravimetric analysis. Biomass & Bioenergy. 27 (4), 385-391. https://doi.org/10.1016/j.biombioe.2003.11.010.
18. Li, H.G., 2005. Principles of Metallurgy. Science Press, Beijing. pp. 291-305.
19. Li, K.Q., Chen, G., Chen, J., Peng, J.H., Ruan, R., Srinivasakannan, C., 2019a. Microwave pyrolysis of walnut shell for reduction process of low-grade pyrolusite. Bioresource Technology. 291, 121838. https://doi.org/10.1016/j.biortech.2019.121838.
20. Li, K.Q., Chen, J., Chen, G., Peng, J.H., Ruan, R., Srinivasakannan, C., 2019b. Microwave dielectric properties and thermochemical characteristics of the mixtures of walnut shell and manganese ore. Bioresource Technology. 286, 121381. https://doi.org/10.1016/j.biortech.2019.121381.
21. Li, K.Q., Chen, G., Li, X.T., Peng, J.H., Ruan, R., Omran, M., Chen, J., 2019c. High-temperature dielectric properties and pyrolysis reduction characteristics of different biomass-pyrolusite mixtures in microwave field. Bioresource Technology. 294, 122217. https://doi.org/10.1016/j.biortech.2019.122217.
22. Li, K.Q., Chen, J., Peng, J.H., Koppala, S., Omran, M., Chen, G., 2020a. One-step preparation of CaO-doped partially stabilized zirconia from fused zirconia. Ceramics International. 46 (6), 6484-6490. https://doi.org/10.1016/j.ceramint.2019.11.129.
23. Li, K.Q., Jiang, Q., Chen, J., Peng, J.H., Li, X.P., Koppala, S., Omran, M., Chen, G., 2020b. The controlled preparation and stability mechanism of partially stabilized zirconia by microwave intensification. Ceramics International. 46 (6), 7523-7530. https://doi.org/10.1016/j.ceramint.2019.11.251.

24. Li, K.Q., Chen, J., Peng, J.H., Ruan, R., Orman, M., Chen, G., 2020c. Dielectric properties and thermal behavior of electrolytic manganese anode mud in microwave field. Journal of Hazardous Materials. 381, 121227. https://doi.org/10.1016/j.jhazmat.2019.121227.

25. Li, K.Q., Jiang, Q., Gao, L., Chen, J., Peng, J.H., Koppala, S., Omran, M., Chen, G., 2020d. Investigations on the microwave absorption properties and thermal behavior of vanadium slag: Improvement in microwave oxidation roasting for recycling vanadium and chromium. Journal of Hazardous Materials. 395, 122698. https://doi.org/10.1016/j.jhazmat.2020.122698.

26. Li, K.Q., Chen, J., Peng, J.H., Omran, M., Chen, G., 2020e. Efficient improvement for dissociation behavior and thermal decomposition of manganese ore by microwave calcination. Journal of Cleaner Production. 260, 121074. https://doi.org/10.1016/j.jclepro.2020.121074.

27. Li, K.Q., Chen, J., Peng, J.H., Ruan, R., Srinivasakannan, C., Chen, G., 2020f. Pilot-scale study on enhanced carbothermal reduction of low-grade pyrolusite using microwave heating. Powder Technology. 360, 846-854. https://doi.org/10.1016/j.powtec.2019.11.015.

28. Liu, Z.W., Zhang, F.X., Liu, H.L., Ba, F., Yan, S.J., Hu, J.H., 2018. Pyrolysis/gasification of pine sawdust biomass briquettes under carbon dioxide atmosphere: Study on carbon dioxide reduction (utilization) and biochar briquettes physicochemical properties. Bioresource Technology. 249, 983-991. https://doi.org/10.1016/j.biortech.2017.11.012.

29. Lu, K.M., Lee, W.J., Chen, W.H., Lin, T.C., 2013. Thermogravimetric analysis and kinetics of co-pyrolysis of raw/torrefied wood and coal blends. Applied Energy. 105, 57-65. https://doi.org/10.1016/j.apenergy.2012.12.050.

30. Ma, Y., Li, S.Y., 2012. The pyrolysis, extraction and kinetics of Buton oil sand bitumen. Fuel Processing Technology. 100, 11-15. https://doi.org/10.1016/j.fuproc.2012.03.001.

31. Mehrabian, R., Scharler, R., Obernberger, I., 2012. Effects of pyrolysis conditions on the heating rate in biomass particles and applicability of TGA kinetic parameters in particle thermal conversion modeling. Fuel. 93, 567-575. https://doi.org/10.1016/j.fuel.2011.09.054.

32. Motasemi, F., Afzal, M.T., 2013. A review on the microwave-assisted pyrolysis technique. Renewable & Sustainable Energy Reviews. 28, 317-330. https://doi.org/10.1016/j.rser.2013.08.008.

33. Song, J.J., Zhu, G.C., Zhang, P., Zhao, Y.N., 2010. Reduction of low-grade manganese oxide ore by biomass roasting. Acta Metallurgica Sinica (English Letters). 23 (3), 223-229. https://doi.org/10.11890/1006-7191-103-223.

34. Sun, J., Wang, W.L, Liu, Z., Ma, Q.L, Zhao, C., Ma, C.Y., 2012. Kinetic study of the pyrolysis of waste printed circuit boards subject to conventional and microwave heating. Energies. 5 (9), 1-12. https://doi.org/10.3390/en5093295.

35. Tilman, D., Hill, J., Lehman, C., 2006. Carbon-negative biofuels from low-input high-diversity grassland biomass. Science. 314 (5805), 1598-1600. https://doi.org/10.1126/science.1133306.

36. Xiang, Z.P., Liang, J.H., Morgan, H.M., Liu, Y.Y., Mao, H.P., Bu, Q., 2018. Thermal behavior and kinetic study for co-pyrolysis of lignocellulosic biomass with polyethylene over Cobalt modified ZSM-5 catalyst by thermogravimetric analysis. Bioresource Technology. 247, 804-811. https://doi.org/10.1016/j.biortech.2017.09.178.

37. Ye, Q.X., Chen, J., Chen, G., Peng, J.H., Srinivasakannan, C., Ruan, R.S., 2018. Effect of microwave heating on the microstructures and kinetics of carbothermal reduction of pyrolusite ore. Advanced Powder Technology. 29 (8), 1871-1878. https://doi.org/10.1016/j.apt.2018.04.025.

38. Ye, Q.X., Zhu, H.B., Zhang, L.B., Liu, P., Chen, G., Peng, J.H., 2014. Carbothermal reduction of low-grade pyrolusite by microwave heating. RSC Advances. 4, 58164-58170. https://doi.org/10.1016/j.jallcom.2014.06.016.

39. Zhao, Y.N., Zhu, G.C., Cheng, Z., 2010. Thermal analysis and kinetic modeling of manganese oxide ore reduction using biomass straw as reductant. Hydrometallurgy. 105 (1-2), 96-102. https://doi.org/10.1016/j.hydromet.2010.08.004.

40. Zhang, H.L., Zhu, G.C., Yan, H., Li, T.C., Zhao, Y., 2013a. The Mechanism on biomass reduction of low-grade manganese dioxide ore. Metallurgical & Materials Transactions B. 44, 889-896. https://doi.org/10.1007/s11663-013-9835-7.

41. Zhang, H.L., Zhu, G.C., Yan, H., Li, T.C., Feng, X.J., 2013b. Thermogravimetric analysis and kinetics on reducing low-grade manganese dioxide ore by biomass. Metallurgical & Materials Transactions B. 44, 878-888. https://doi.org/10.1007/s11663-013-9840-x.

42. Zhang, X.S., Lei, H.W., Chen, S.L., Wu, J.A., 2016. Catalytic co-pyrolysis of lignocellulosic biomass with polymers: a critical review. Green chemistry. 18, 4145-4169. https://doi.org/10.1039/C6GC00911E.

Table captions

Table 1 Component analysis of low-grade pyrolusite.

Table 2 Ultimate and proximate analysis of walnut shell.

Table 3 Comparison of the maximum relative error at 400 °C-600 °C between the experimental and calculated TGA curves of five walnut shell-pyrolusite blends.

Table 4 Comparison of residue between the experimental and calculated TGA curves of five walnut shell-pyrolusite blends.

Table 5 Kinetics parameters of reducing low-grade pyrolusite by walnut shell.

Figure captions

Fig.1. Reduction ratios of low-grade pyrolusite reducing by walnut shell under microwave heating at different experimental conditions.

Fig.2. Fitting curves between different kinetic equations and time, (a)-(b) chemical reaction control; (c)-(d) external diffusion control; (e)-(f) internal diffusion control.

Fig.3. TGA-DTG curves of low-grade pyrolusite (a) and walnut shell (b).

Fig.4. TGA-DTG curves of five walnut shell-pyrolusite blends at different mixing ratios, (a) 1.2: 10; (b) 1.4: 10; (c) 1.6: 10; (d) 1.8: 10; (e) 2.0: 10.

Fig.5. ΔW variation of TGA-DTG curves of five walnut shell-pyrolusite blends at different mixing ratios, (a) TGA curves; (b) DTG curves.

Fig.6. Plot of $\ln[\frac{-\ln(1-X)}{T^2}]$ against 1/T for reducing low-grade pyrolusite by walnut shell with different mixing ratios, (a) 1.2:10; (b) 1.4:10; (c) 1.6:10; (d) 1.8:10; (e) 2.0:10.

Table 1 Component analysis of low-grade pyrolusite

Compositions	T_{Mn}	Mn^{4+}	Mn^{2+}	Fe^{3+}	Al_2O_3
Mass (w%)	28.81	26.03	1.28	7.76	2.52
Compositions	CaO	MgO	SiO_2	P	S
Mass (w%)	1.24	1.16	25.83	0.14	0.27

Table 2 Ultimate and proximate analysis of walnut shell (%)

Ultimate analysis					Proximate analysis			
C	H	O	N	S	Moisture	Volatiles	Fixed carbon	Ash
48.34	6.03	43.24	1.028	0.14	6.23	69.72	21.06	2.99

Table 3 Comparison of the maximum relative error at 400 °C-600 °C between the experimental and calculated TGA curves of five walnut shell-pyrolusite blends

Mixing ratio	10:1.2	10:1.4	10:1.6	10:1.8	10:2.0
Temperature (°C)	522.4	524.0	536.0	535.8	535.9
Experiment (wt%)	83.168	80.361	79.664	80.709	79.164
Calculation (wt%)	86.889	85.837	84.596	83.648	82.726
Relative error (%)	4.474	6.814	6.191	3.641	4.500

Table 4 Comparison of residue between the experimental and calculated TGA curves of five walnut shell-pyrolusite blends

Mixing ratio	10:1.2	10:1.4	10:1.6	10:1.8	10:2.0
Experiment (wt%)	77.440	74.003	73.727	74.413	73.406
Calculation (wt%)	82.343	81.307	80.306	79.339	78.404
Relative error (%)	6.331	9.870	8.923	6.620	6.809

Table 5 Kinetics parameters of reducing low-grade pyrolusite by walnut shell

Mixing ratio	Temperature (°C)	E_a (kJ·mol^{-1})	A (min^{-1})	R^2	R
10:1.2	250~400	16.68	4.10E-01	0.99672	0.998
10:1.4	250~400	15.45	3.61E-01	0.99649	0.998
10:1.6	250~400	13.51	2.30E-01	0.99504	0.998
10:1.8	250~400	5.62	4.26E-02	0.99659	0.998
10:2.0	250~400	16.69	5.15E-01	0.99702	0.999

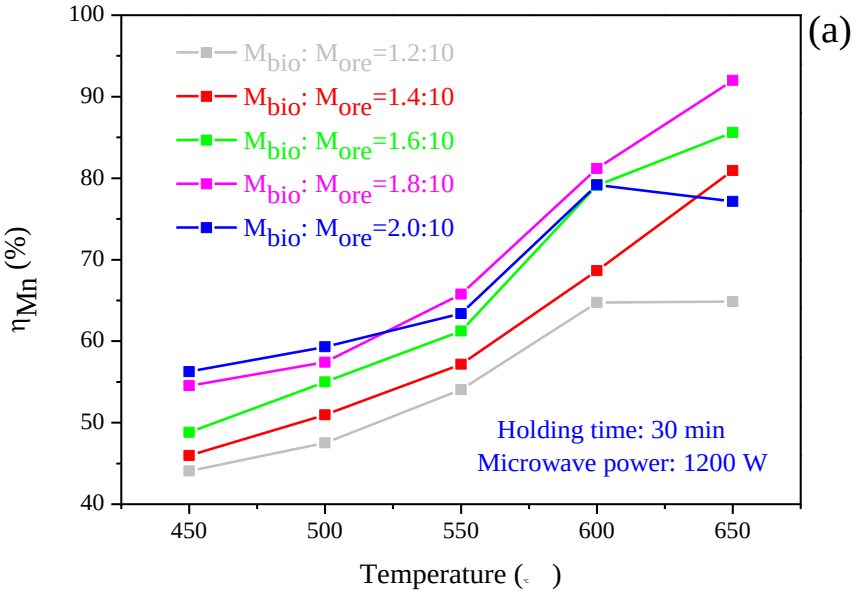
(a)
M_{bio}: M_{ore}=1.2:10
M_{bio}: M_{ore}=1.4:10
M_{bio}: M_{ore}=1.6:10
M_{bio}: M_{ore}=1.8:10
M_{bio}: M_{ore}=2.0:10
Holding time: 30 min
Microwave power: 1200 W
η_{Mn} (%)
Temperature (℃)

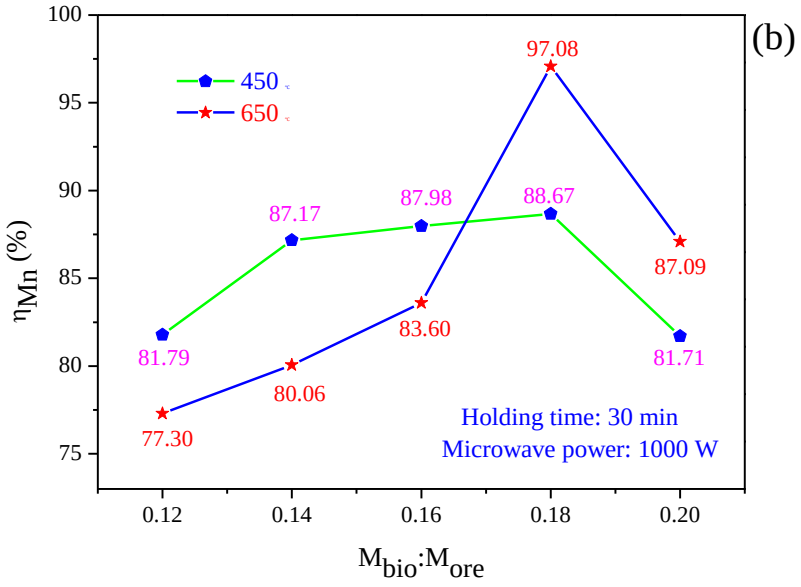
(b)
450 ℃
650 ℃
97.08
87.17
87.98
88.67
87.09
83.60
81.79
80.06
81.71
77.30
Holding time: 30 min
Microwave power: 1000 W
η_{Mn} (%)
M_{bio}:M_{ore}

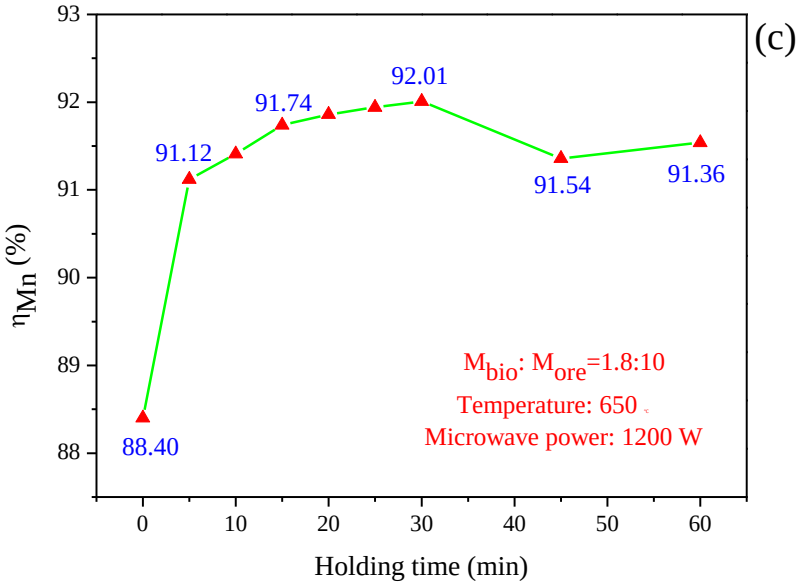
(c)
92.01
91.74
91.12
91.54
91.36
88.40
M_{bio}: M_{ore}=1.8:10
Temperature: 650 ℃
Microwave power: 1200 W
η_{Mn} (%)
Holding time (min)

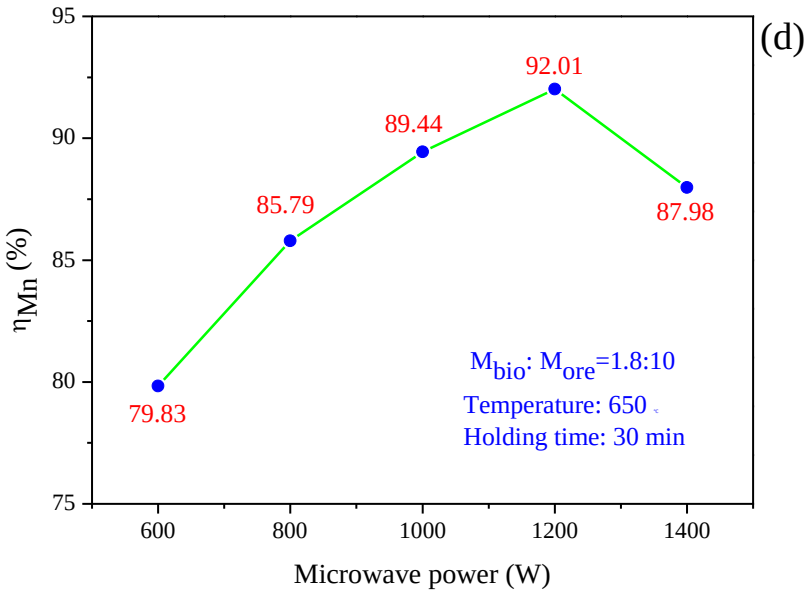

Fig. 1. Reduction ratios of low-grade pyrolusite reducing by walnut shell under microwave heating at different experimental conditions.

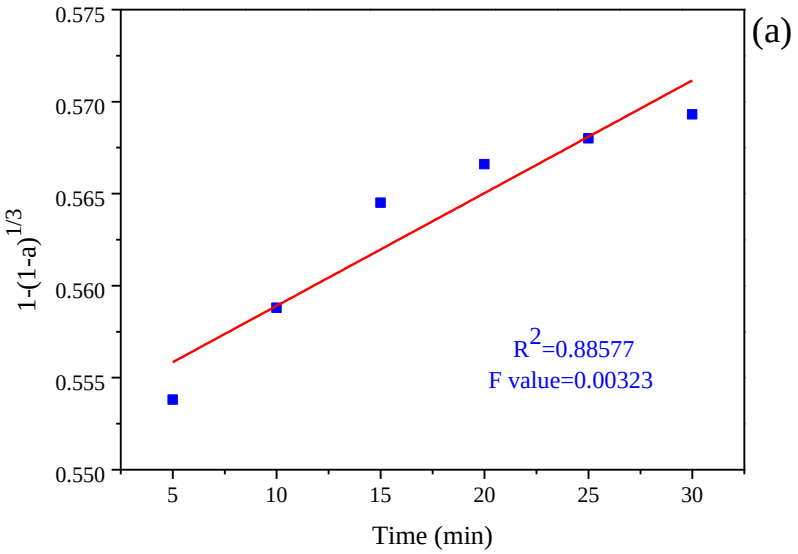
(a)
0.575
0.570
0.565
0.560
0.555
0.550
1-(1-a)^1/3
R^2=0.88577
F value=0.00323
5
10
15
20
25
30
Time (min)

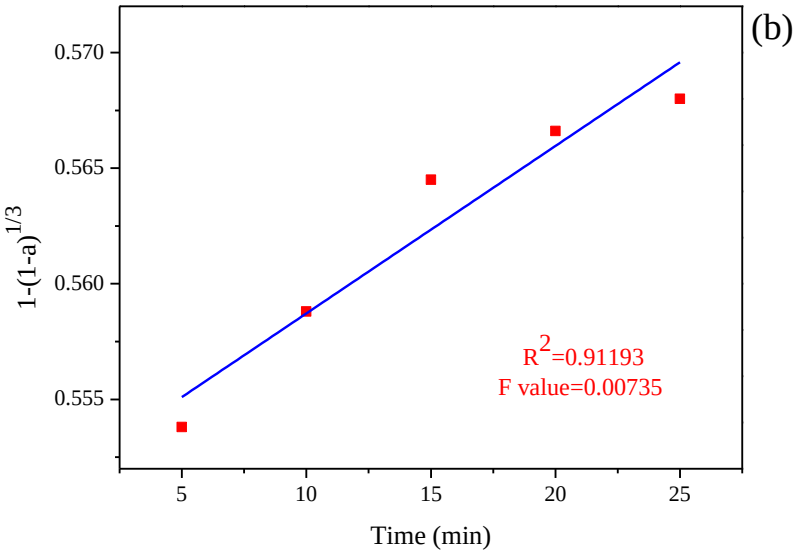
(b)
0.570
0.565
0.560
0.555
1-(1-a)^1/3
R^2=0.91193
F value=0.00735
5
10
15
20
25
Time (min)

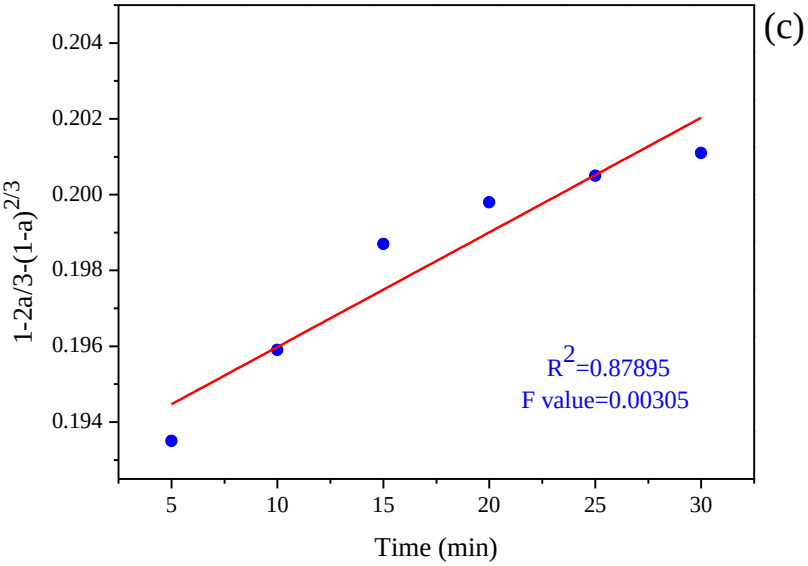
(c)
0.204
0.202
0.200
0.198
0.196
0.194
1-2a/3-(1-a)^2/3
R^2=0.87895
F value=0.00305
5
10
15
20
25
30
Time (min)

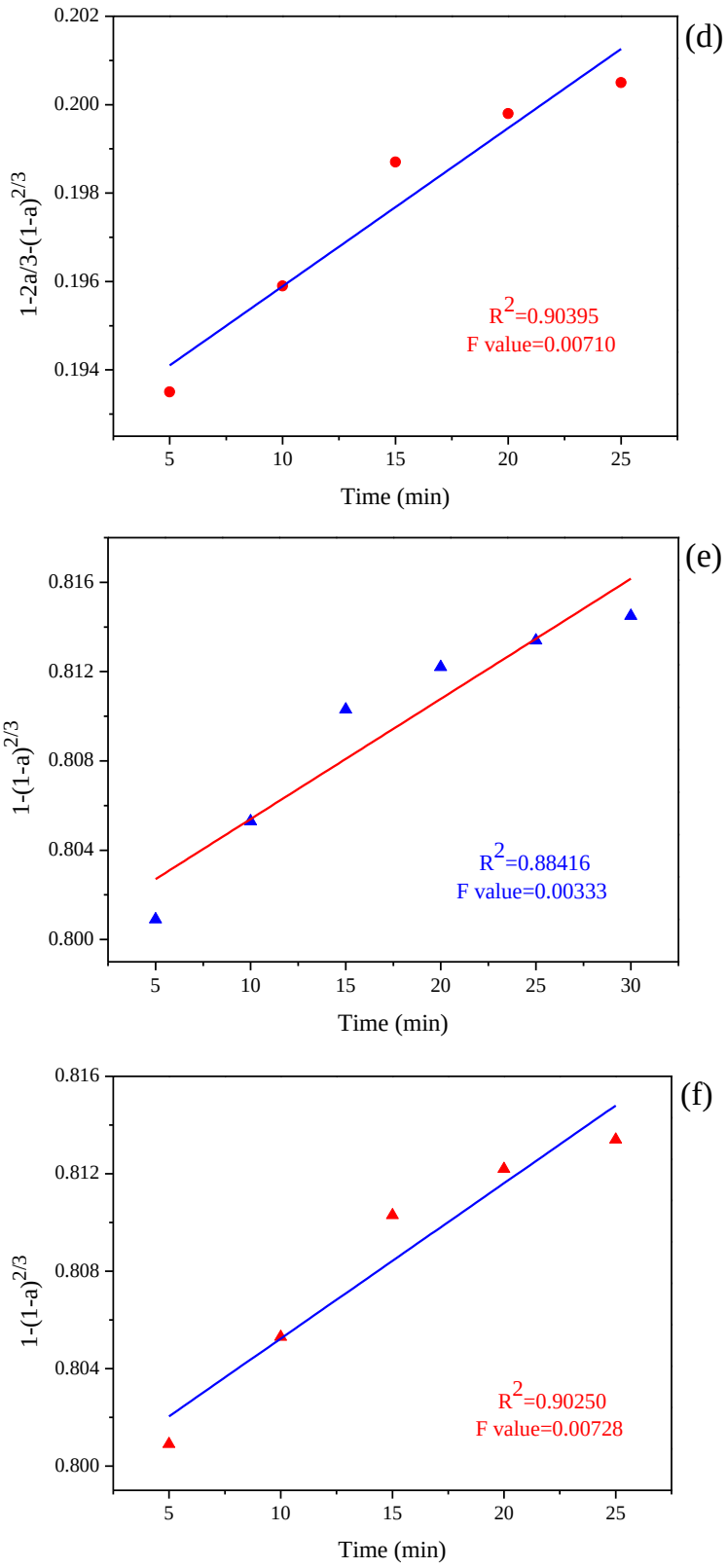

Fig. 2 Fitting curves between different kinetic equations and time, (a)-(b) chemical reaction control; (c)-(d) external diffusion control; (e)-(f) internal diffusion control.

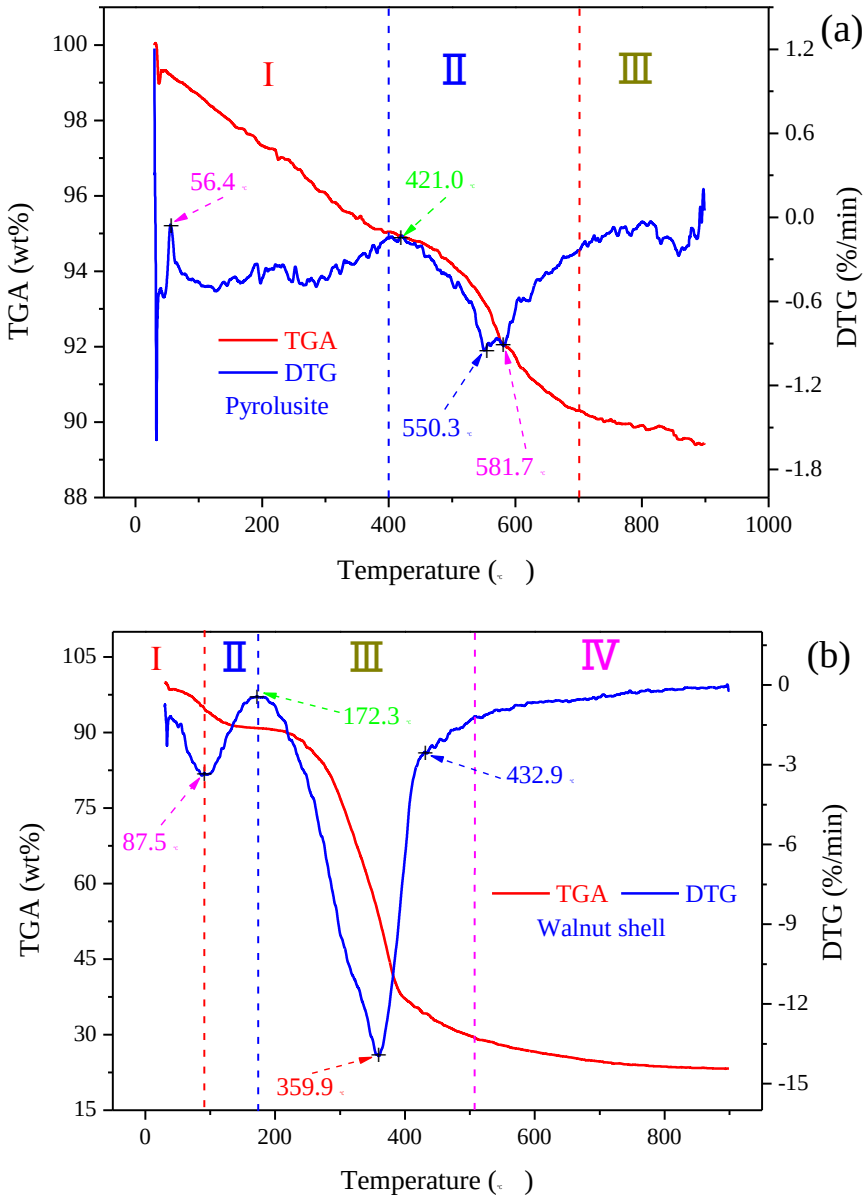

Fig. 3 TGA-DTG curves of low-grade pyrolusite (a) and walnut shell (b).

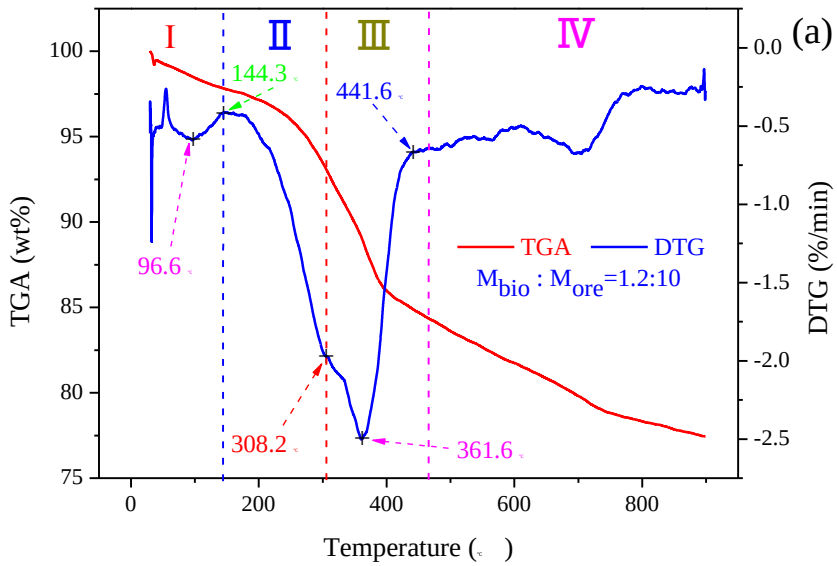
I
II
III
IV
(a)
144.3
441.6
96.6
308.2
361.6
TGA
DTG
M_{bio} : M_{ore}=1.2:10
TGA (wt%)
DTG (%/min)
Temperature (°C)

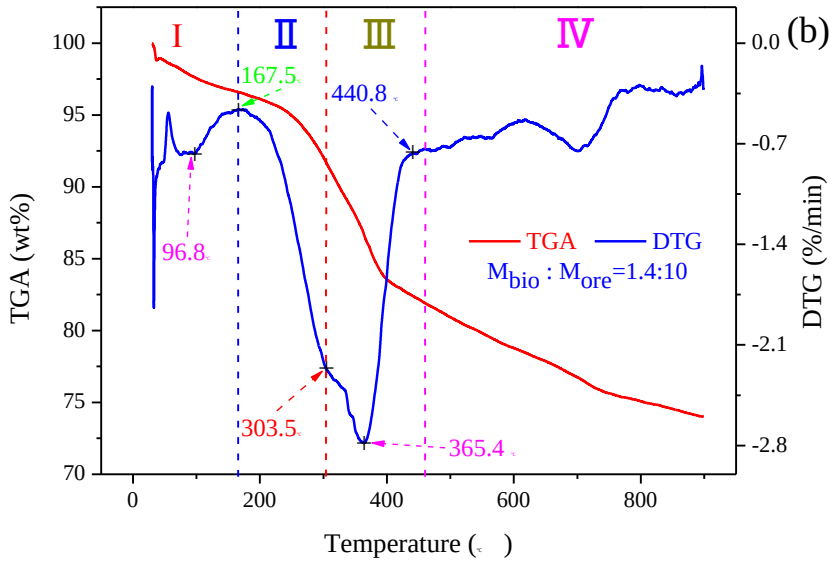
I
II
III
IV
(b)
167.5
440.8
96.8
303.5
365.4
TGA
DTG
M_{bio} : M_{ore}=1.4:10
TGA (wt%)
DTG (%/min)
Temperature (°C)

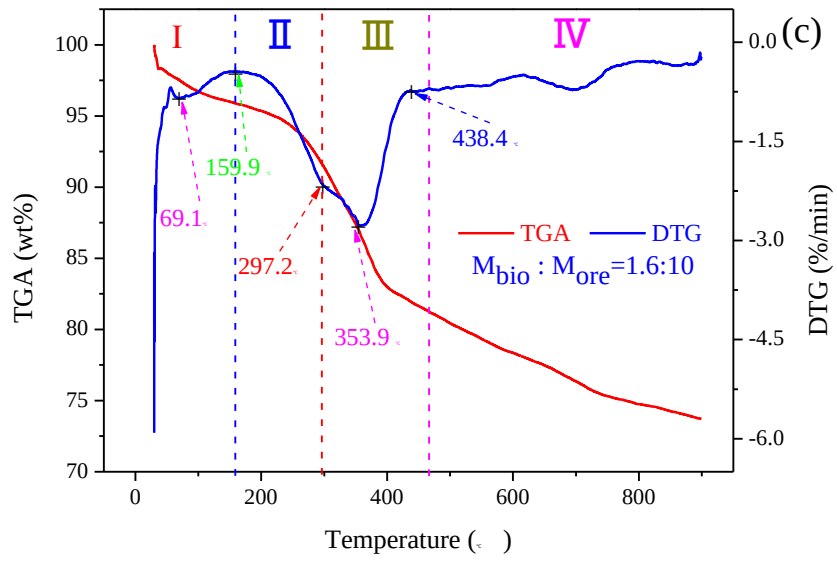
I
II
III
IV
(c)
438.4
159.9
69.1
297.2
353.9
TGA
DTG
M_{bio} : M_{ore}=1.6:10
TGA (wt%)
DTG (%/min)
Temperature (°C)

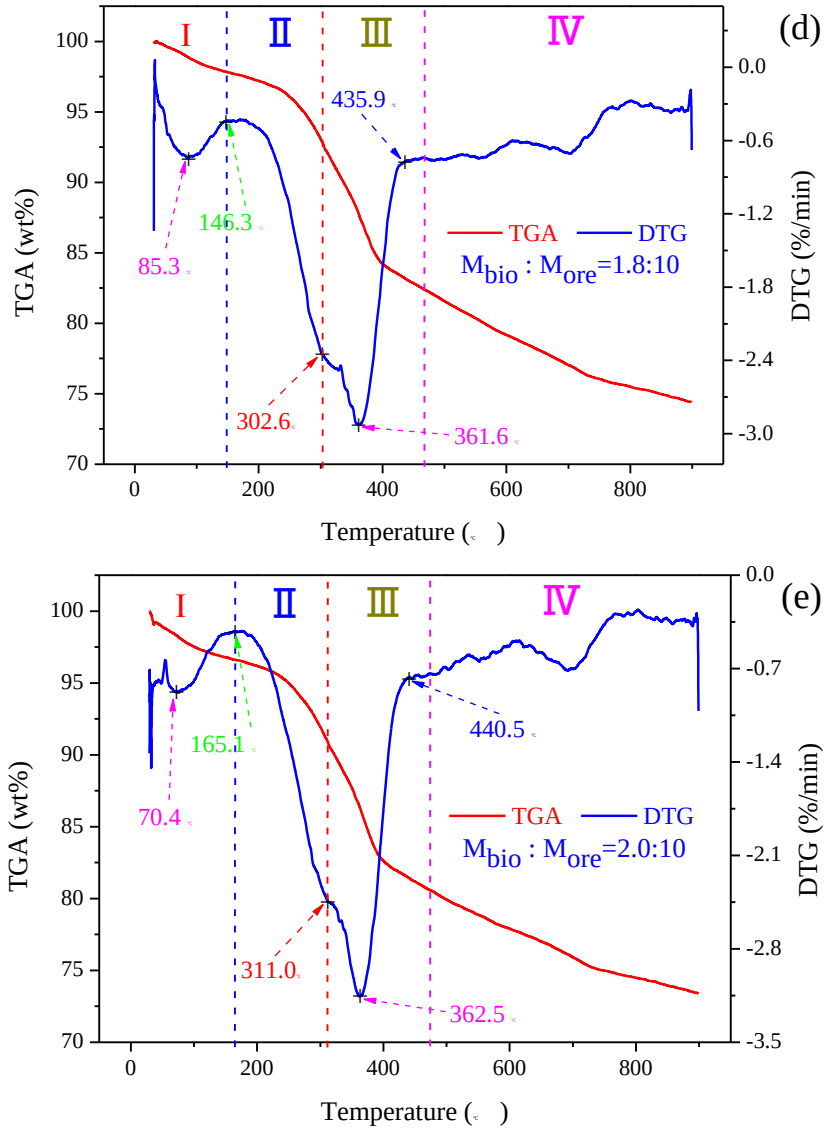

Fig. 4 TGA-DTG curves of five walnut shell-pyrolusite blends at different mixing ratios, (a) 1.2:10; (b) 1.4:10; (c) 1.6:10; (d) 1.8:10; (e) 2.0:10.

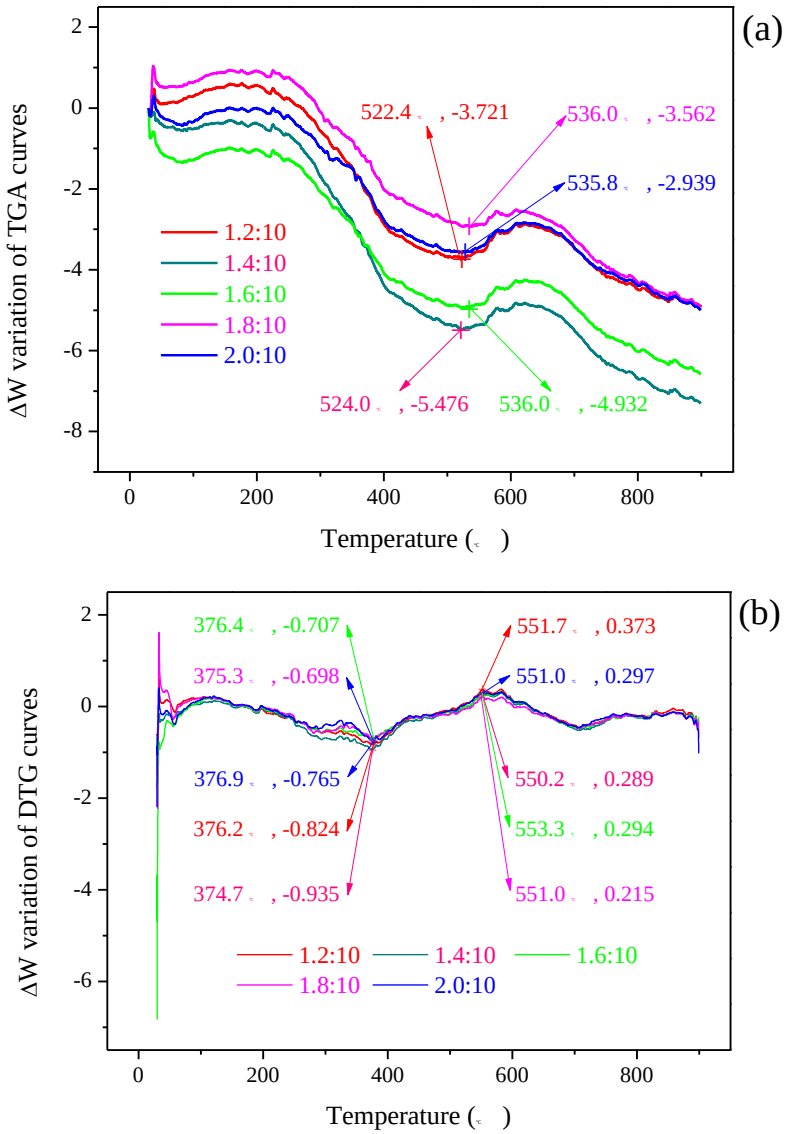

Fig. 5 ΔW variation of TGA-DTG curves of five walnut shell-pyrolusite blends at different mixing ratios, (a) TGA curves; (b) DTG curves.

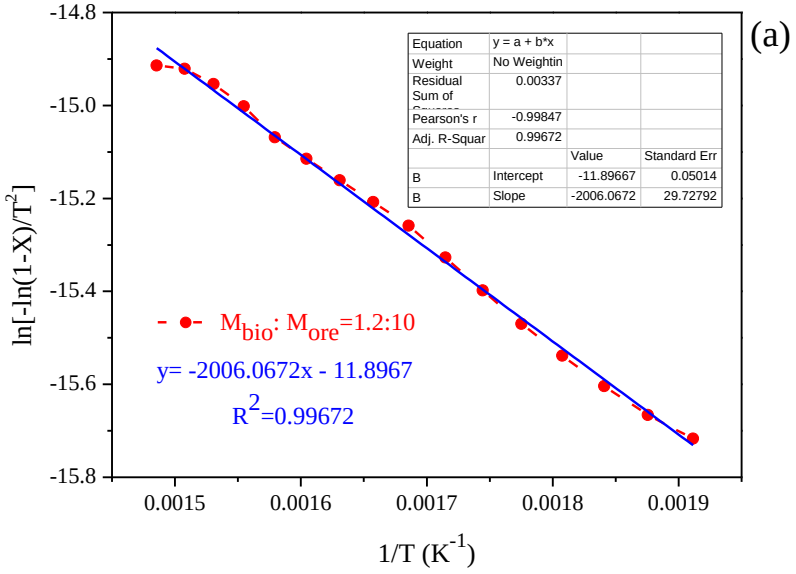
(a)
ln[-ln(1-X)/T²]
1/T (K⁻¹)
Equation y = a + b*x
Weight No Weightin
Residual Sum of 0.00337
Pearson's r -0.99847
Adj. R-Squar 0.99672
Value Standard Err
B Intercept -11.89667 0.05014
B Slope -2006.0672 29.72792
Mbio: More=1.2:10
y= -2006.0672x - 11.8967
R²=0.99672

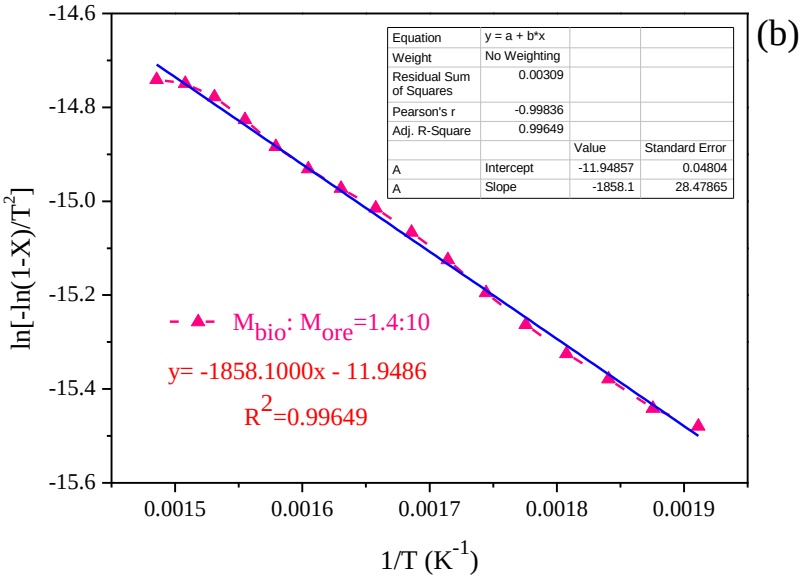
(b)
ln[-ln(1-X)/T²]
1/T (K⁻¹)
Equation y = a + b*x
Weight No Weighting
Residual Sum of Squares 0.00309
Pearson's r -0.99836
Adj. R-Square 0.99649
Value Standard Error
A Intercept -11.94857 0.04804
A Slope -1858.1 28.47865
Mbio: More=1.4:10
y= -1858.1000x - 11.9486
R²=0.99649

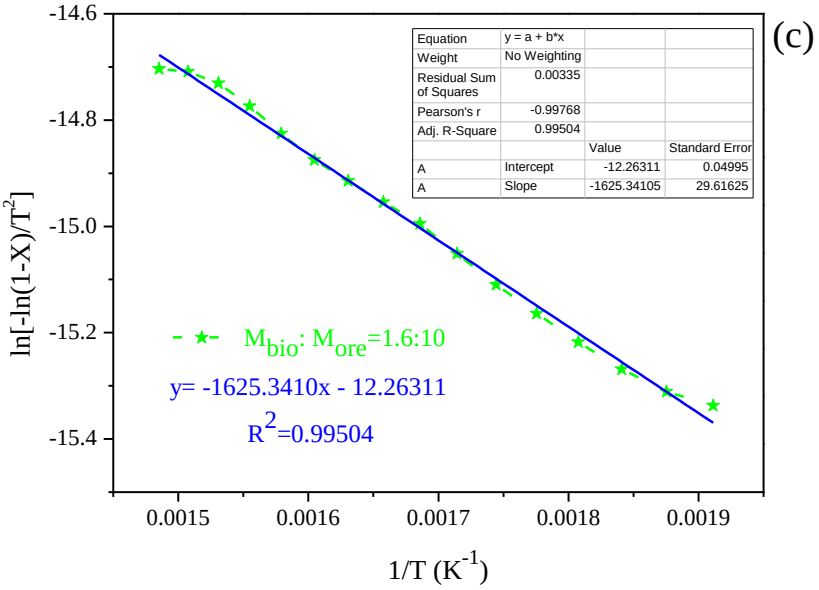
(c)
ln[-ln(1-X)/T²]
1/T (K⁻¹)
Equation y = a + b*x
Weight No Weighting
Residual Sum of Squares 0.00335
Pearson's r -0.99768
Adj. R-Square 0.99504
Value Standard Error
A Intercept -12.26311 0.04995
A Slope -1625.34105 29.61625
Mbio: More=1.6:10
y= -1625.3410x - 12.26311
R²=0.99504

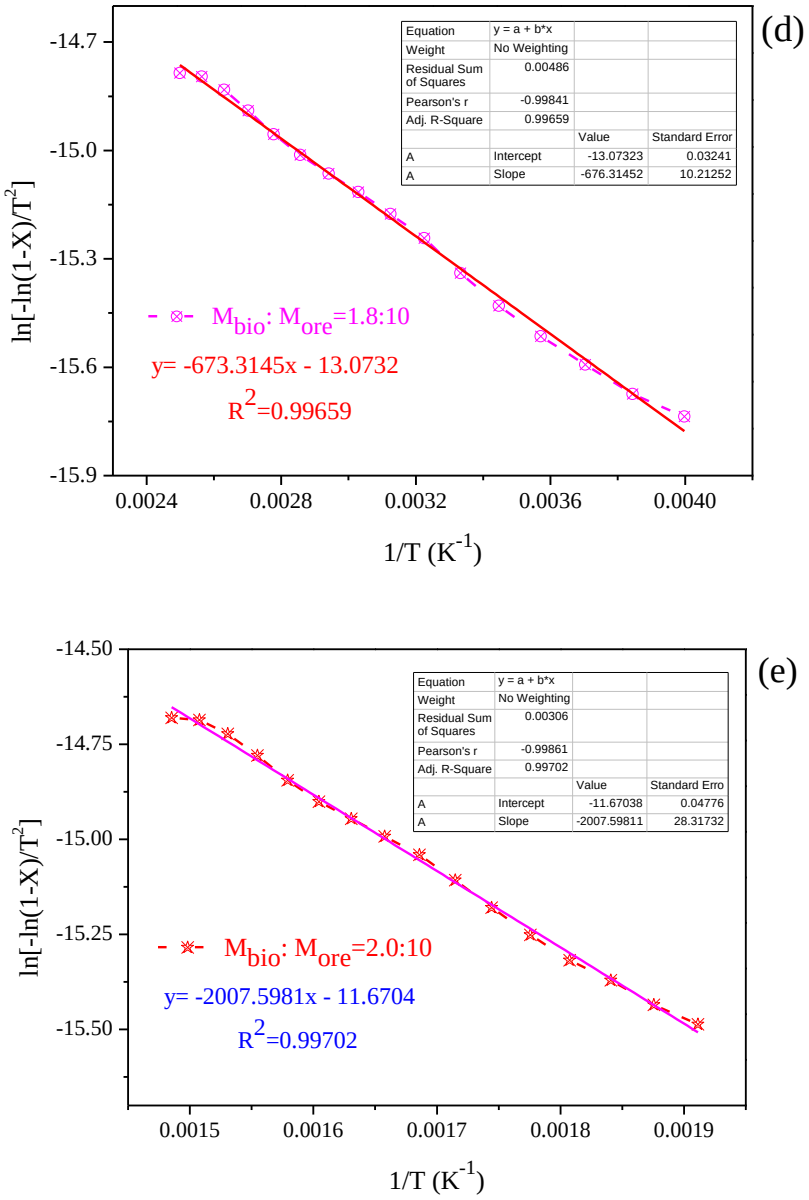

Fig. 6 Plot of $\ln[\frac{-\ln(1-X)}{T^2}]$ against 1/T for reducing low-grade pyrolusite by walnut shell with different mixing ratios, (a) 1.2:10; (b) 1.4:10; (c) 1.6:10; (d) 1.8:10; (e) 2.0:10.

Declaration of interests

☒ The authors declare that they have no known competing financial interests or personal relationships that could have appeared to influence the work reported in this paper.

☐The authors declare the following financial interests/personal relationships which may be considered as potential competing interests: